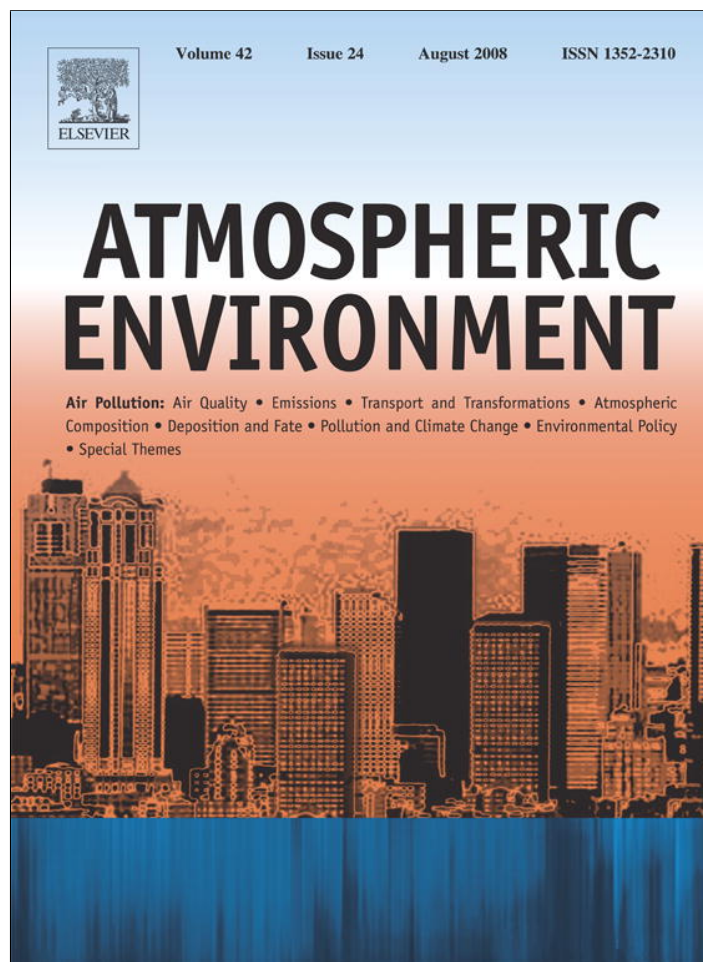


Provided for non-commercial research and education use.  
Not for reproduction, distribution or commercial use.



This article appeared in a journal published by Elsevier. The attached copy is furnished to the author for internal non-commercial research and education use, including for instruction at the authors institution and sharing with colleagues.

Other uses, including reproduction and distribution, or selling or licensing copies, or posting to personal, institutional or third party websites are prohibited.

In most cases authors are permitted to post their version of the article (e.g. in Word or Tex form) to their personal website or institutional repository. Authors requiring further information regarding Elsevier's archiving and manuscript policies are encouraged to visit:

<http://www.elsevier.com/copyright>



# Long-range transport of acidifying substances in East Asia—Part I Model evaluation and sensitivity studies

Meiyun Lin<sup>a,\*</sup>, Taikan Oki<sup>a</sup>, Tracey Holloway<sup>b</sup>, David G. Streets<sup>c</sup>,  
Magnus Bengtsson<sup>d</sup>, Shinjiro Kanae<sup>a</sup>

<sup>a</sup>*Institute of Industrial Science, University of Tokyo, Tokyo, Japan*

<sup>b</sup>*Center for Sustainability and the Global Environment, University of Wisconsin-Madison, WI, USA*

<sup>c</sup>*Argonne National Laboratory, Argonne, IL, USA*

<sup>d</sup>*Institute for Global Environmental Strategies, Kanagawa, Japan*

Received 22 November 2007; received in revised form 4 April 2008; accepted 18 April 2008

## Abstract

This study has conducted a comprehensive model evaluation to help identify major uncertainties of regional air quality model in predicting long-range transport and deposition of acidifying substances in East Asia. Annual predictions of the Community Multiscale Air Quality (CMAQ) model are carried out at two horizontal scales: an 81 km domain over East Asia and a 27 km domain over Northeast Asia. The model successfully reproduces the magnitudes and diurnal variations of SO<sub>2</sub> mixing ratios at most sites of the Acid Deposition Monitoring Network in East Asia (EANET). Through the comparison with tropospheric NO<sub>2</sub> columns from the Global Ozone Monitoring Experiment (GOME), the model is shown to be able to capture major spatial and seasonal variations of NO<sub>2</sub> observed from space over East Asia. Regarding the magnitudes, however, CMAQ underpredicts the GOME retrieval over industrial area of eastern China in March and December, and over the remote western China in July. Primary reasons for the discrepancy over eastern China are the uncertainties both in emission inventory and in the GOME retrieval in wintertime. For the wet season the soil-biogenic NO emission estimates need to be reviewed regarding the intensity and timing of fertilizer applications, and the magnitude of rain-induced pulsing. The sensitivities of predicted NO<sub>2</sub> columns, NO<sub>x</sub> mixing ratios, and wet nitrate deposition to 50% increase of NO<sub>x</sub> emissions are studied. Due to the underpredictions of NO<sub>x</sub> and also to the uncertainty in modeled precipitation and nitrate formation, CMAQ has a tendency to underpredict annual wet deposition loads of nitrate observed by the EANET network.

© 2008 Elsevier Ltd. All rights reserved.

**Keywords:** Nitrogen oxides; Satellite data; Acid deposition; Multiscale; East Asia

## 1. Introduction

Nitrogen oxides (NO<sub>x</sub> = NO + NO<sub>2</sub>) are emitted into the atmosphere by natural processes such as lightning or soil emissions, and by human activities

\*Corresponding author. Tel.: +81 3 5452 6382;  
fax: +81 3 5452 6383.

E-mail address: [lin@rainbow.iis.u-tokyo.ac.jp](mailto:lin@rainbow.iis.u-tokyo.ac.jp) (M. Lin).

related to power generation, industry, traffic, and open biomass burning. Emissions of  $\text{NO}_x$  over Asia have experienced a rapid increase in the last decade (Naja and Akimoto, 2004), with China and India being the largest contributors. Richter et al. (2005) have reported that the vertical column densities (VCDs) of tropospheric  $\text{NO}_2$  in satellite measurements over the industrial area of China increased about 50% from 1996 to 2004 with an accelerating trend in annual growth rate. The principal sink of tropospheric  $\text{NO}_x$  is oxidation to nitric acid ( $\text{HNO}_3$ ) by reaction of  $\text{NO}_2$  with OH during daytime and by reaction of  $\text{NO}_2$  with ozone ( $\text{O}_3$ ) followed by hydrolysis of  $\text{N}_2\text{O}_5$  on aerosols at night (Dentener et al., 1993; Evans and Jacob, 2005). Recent ground-based monitoring data indicate that the relative contribution of  $\text{HNO}_3$  to the precipitation acidity in parts of East Asia is gradually increasing (e.g. Seto et al., 2002; Xie, 2002).

The long-range transport and fate of Asian pollutants in the atmosphere is an area of increasing scientific interest and political concern. Hemispheric transport of CO and  $\text{O}_3$  have been examined through global chemical transport modeling and analysis of ozone soundings (e.g. Liu et al., 2002; Naja and Akimoto, 2004) and aircraft measurements (e.g. Bey et al., 2001). A large set of global chemical transport models (CTMs) has been used to discuss the relationship between  $\text{NO}_x$  emissions and satellite  $\text{NO}_2$  VCDs (e.g. van Noije et al., 2006; Wang et al., 2007; Martin et al., 2007). These global scale studies will be useful for assessing regional air quality, but they do not replace the need for regional scale analysis. Regional CTMs are needed to estimate source–receptor (S/R) relationships at regional scales, and to examine pollution and precursor outflow to other areas (Carmichael et al., 2007). Due to lack of measurement data, one of the key problems of regional air quality modeling in East Asia is reducing the uncertainties in the boundary conditions (BCs). By linking a global CTM to regional modeling in East Asia, the present study seeks to quantify the impact of global inflows as well as regional sources on the deposition load of sulfur and reactive nitrogen in East Asia. The state-of-the-art regional Community Multiscale Air Quality model (CMAQ v4.5.1) (Byun and Ching, 1999; Byun and Schere, 2006) is employed at two horizontal scales: a 81 km domain over East Asia and a nested 27 km domain over Northeast Asia. To suppress the inaccuracy of lateral-fixed BC and also to quantify the global inflows, the global

Model for Ozone and Related Chemical Tracers (MOZART v2.4) (Horowitz et al., 2003) is coupled to provide BCs for the 81 km domain of CMAQ. In addition, we have developed a new emission processing model to incorporate various emission data with different resolutions to the uniform model grids.

To support the application of the multiscale model system to predict S/R relationships, a comprehensive model evaluation has been carried out by using in situ monitoring and satellite measurements. We present our results of model evaluation and S/R relationships for acidifying substances as two parts. The current paper, Part I, describes the modeling system and presents the evaluation of CMAQ annual predictions with ground-based data from the Acid Deposition Monitoring Network in East Asia (EANET) (EANET, 2002), and with satellite data from the Global Ozone Monitoring Experiment (GOME) instrument (Richter et al., 2005). The Part II paper (Lin et al., 2008b) presents the results of source region attribution for sulfur and reactive nitrogen deposition in East Asia. In addition, we have also employed the same models to examine the budget and photochemical sensitivity of  $\text{O}_3$  production, which is presented in a separate paper (Lin et al., 2008a).

The current paper is structured as follows. Section 2 provides a brief overview of CMAQ v4.5.1 and related data including emissions, meteorology, BCs, and observations. Section 3 evaluates spatial, seasonal, and diurnal variations of primary gas  $\text{SO}_2$  with the EANET surface measurements. Section 4 presents an integrated evaluation of tropospheric  $\text{NO}_2$  columns and surface  $\text{NO}_x$  concentrations by using the combination of in situ and satellite measurements. Section 5 analyzes the chemical components in rainwater and the deposition load of sulfate, nitrate and ammonium.

## 2. Data and methods

### 2.1. Model setup and meteorological inputs

CMAQ v4.5.1 contains several updates from the previous release of the model. A new global mass continuity scheme is implemented. This scheme is globally mass-conserving and uses the piecewise parabolic method (PPM) (Colella and Woodward, 1984) advection scheme for horizontal advection. The minimum value for the eddy diffusivity ( $K_z$ ) has

an important impact on nighttime concentrations. A new option for minimum  $K_z$  is introduced in CMAQ v4.5.1. The new version interpolates between urban and non-urban land cover to calculate minimum  $K_z$  which can vary from 0.5 to 2.0 m<sup>2</sup> s<sup>-1</sup>. Gas-phase chemistry is simulated with the Carbon-Bond IV (CBIV) (Gery et al., 1989) mechanism with the Euler Backwards Iterative (EBI) solver. CMAQ is configured with the AERO-3 aerosol module (Binkowski and Roselle, 2003), in which sea salt and the interactions between the fine- and coarse-mode particles are not treated.

The study region is centered at (110°E, 20°N) on a Lambert projected map of East Asia (Fig. 1). The modeling domains consist of a coarse 81 km domain that covers the wide areas of East Asia and a one-way nested 27 km domain that covers an area of Northeast Asia including central east China, the Korea Peninsula, and Japan. The meteorological fields for both domains are generated by the MM5 model (Grell et al., 1994) with four-dimensional data assimilation. MM5 initialization uses the NCEP/NCAR global meteorological reanalysis data sets (6 h interval and 2.5 × 2.5° resolution). A three-dimensional (3-D) grid nudging technique (6 h interval) is used both for the coarse- and fine-grid simulations. No surface nudging is performed. The Noah land surface model was adopted to simulate land surface interactions, the cloud scheme of Grell et al. (1994) was chosen for the physical parameterization, and the MRF scheme of Hong

and Pan (1996) was employed for planetary boundary layer (PBL) parameterization. A spin-up period of two months (November–December 2000) is carried out to allow clouds and other process to spin up in MM5. We find that the spin-up process significantly improves the simulated precipitation in Southeast Asia during the beginning three months of 2001.

There are 23 sigma levels from surface to 15 km for the MM5 meteorological predictions. The MM5 output files are post-processed with the Meteorology-Chemistry Interface Processor (MCIP) version 3.0 for CMAQ. In order to alleviate the computational cost of CMAQ for S/R calculations associated with a large number of vertical layers, vertical layer collapsing is performed to reduce the vertical layers from 23 MM5 sigma levels to nine sigma levels in CMAQ with a fine resolution in the PBL. The CMAQ layers correspond to sigma levels of 1.00, 0.98, 0.96, 0.92, 0.88, 0.80, 0.60, 0.30, and 0.00. The height of first CMAQ layer is set to 73 m, which was also used in the Chemical Weather Forecasting System (CFORS) (Carmichael et al., 2003) and was shown to be robust for regional scale studies. The intercomparison study of tropospheric NO<sub>2</sub> columns from 17 global models with vertical layers ranging from 19 levels to 52 levels (van Noije et al., 2006) suggested that the model derived NO<sub>2</sub> vertical columns are not sensitive to model vertical resolutions.

## 2.2. Emission data

Emission data applied in this study include anthropogenic, biomass burning, volcanic SO<sub>2</sub>, and biogenic emissions. Anthropogenic emissions of SO<sub>2</sub>, NO<sub>x</sub>, NH<sub>3</sub>, CO and VOCs (volatile organic compounds) were taken from Streets et al. (2003a) derived for the TRACE-P experiment as well as emission database for global atmospheric research (Olivier et al., 2005) over regions for which TRACE-P estimates are unavailable. The TRACE-P inventory investigated the monthly variation of emissions of the major species at provincial scale in China. This addressed additional emissions during the winter heating season in China and the greater intensity of evaporative emissions (NH<sub>3</sub> and CH<sub>4</sub>) during the warmer months. Biomass burning emissions with seasonal and inter-annual variability were taken from van der Werf et al. (2006). The SO<sub>2</sub> emissions from the largest erupting volcano of Miyakejima, located to the south of Tokyo, were taken from Kajino et al. (2004) and Kazahaya et al. (2004). Seasonal emission

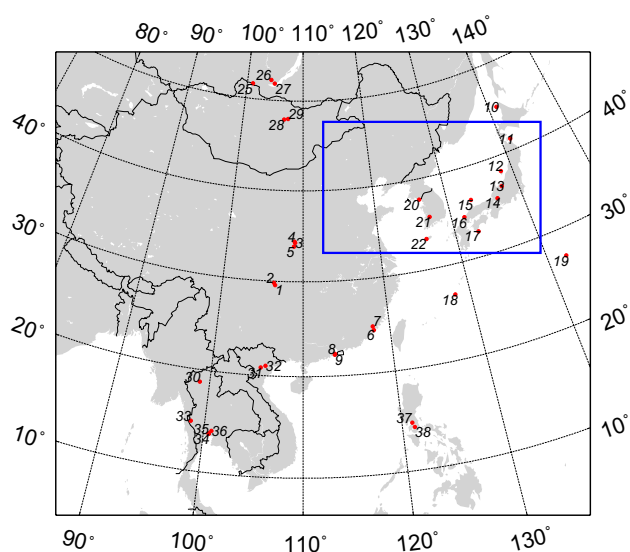


Fig. 1. Model domains (81-km and 27-km horizontal resolution) for the application of CMAQ in East Asia. Locations of EANET monitoring sites are also shown.

flux of NO from soils (Yienger and Levy, 1995) as well as CO and hydrocarbons (i.e. isoprene, monoterpene, and acetone) from vegetation in the year 2000 were obtained from Olivier et al. (2003). It should be noted that emissions of lightning produced NO<sub>x</sub>, wind blown sea salt and dust are not included currently since the influence of anthropogenic sources to acid deposition is the primary focus of this study. The exclusion of these emissions is assumed not to have significant influence on the results of S/R relationships for acid deposition.

The widely used SMOKE emission processing model requires a large set of surrogate data and sector/regional dependent temporal profiles. These data are probably not available in regions other than North America. Thus, we have developed a new emission processing model to import and transform aforementioned inventory data by gridded emission control (for S/R perturbation runs), spatial interpolation, temporal allocation, and chemical speciation. This new model is an effective alternative to the SMOKE model, and is well suited for adapting existing emission data in regions other than North America. The new emission processing model is publicly available upon request.

For the current study, inventory data with different spatial resolutions are sampled and interpolated to the model grids of 81- and 27-km, respectively. All large point sources (LPS) are injected into model layers according to stack parameters, with the stack height of volcanoes assumed to be 1500 m and anthropogenic LPSs (power plants and large industries) assumed to be 300 m. It is assumed that 90% of anthropogenic NO<sub>x</sub> emissions are in the form of NO and 10% in the form of NO<sub>2</sub>. For VOCs speciation, firstly the national (provincial scale in China) speciation profiles from the TRACE-P inventory are allocated to each grid cell based on grid region ID. Secondly, the gridded speciation profiles are used to split VOCs emissions into individual pollutants. Thirdly, the mechanism dependent speciation profiles (information available at <http://pah.cert.ucr.edu/~carter/emitdb/emitdb.xls>) are imported to lump the inventory pollutants to the photochemical species of CBIV. For the speciation of primary particulate matters (PM<sub>2.5</sub>), the mass ratios of primary sulfate and nitrate are assumed to be 18% and 8%, respectively, for fossil fuel burning, while 1% and 0.3% for biofuel fuel or biomass burning (Wang et al., 2006). The chemical processing module included in the emission model is general

to work for the CBIV, SAPRC99 (Carter, 2000), and other user-defined mechanisms.

### 2.3. Initial and boundary conditions

Initial conditions for the 81 km domain of CMAQ use the default concentration profiles which are intended to represent relatively clean air conditions. A spin-up period of two weeks (15 December 2000–1 January 2001) is used to minimize the influences of initial conditions. CMAQ with the 81-km grid spacing is then continuously run from January to December in 2001.

Driving regional CTMs with BCs derived from global models tends to provide more realistic spatial and temporal variability than with the lateral-fixed profiles. In this study we adopted monthly mean results of the global model MOZART to provide BCs for the CMAQ 81 km domain. In addition, the CMAQ 27 km simulation adopted hourly varying BCs derived from the CMAQ coarse simulations. The hourly varying BCs intend to provide more realistic temporal variability than monthly mean BCs from MOZART. The MOZART simulations were driven with NCEP reanalysis meteorology for 2000–2002 and were evaluated in Holloway et al. (2007). Horizontal interpolation and vertical linear interpolation based on layer height are carried out to convert data on the MOZART coordinate ( $1.9 \times 1.9^\circ$ , 28 vertical hybrid sigma levels) to the CMAQ coordinate (81 × 81 km, eight vertical  $\sigma_p$  layers). The MOZART outputs for BCs consisted of 19 species including O<sub>3</sub>, peroxyacetyl nitrate (PAN), long-lived hydrocarbons, aerosols, and other gases. It should be noted that CMAQ uses lateral BCs only. No upper BCs of O<sub>3</sub> are employed in CMAQ.

### 2.4. Observation data

Table 1 and Fig. 1 give the location and characteristics of EANET monitoring sites, labeled by identification numbers in comparison figures. Automatic monitoring method is used for the hourly air concentration data in Japan. For wet deposition, precipitation samples were collected using a wet-only sampler on a daily basis for most sites and on a weekly basis for the sites in Philippines and Vietnam (EANET, 2002). Ion chromatography is a major analytical method for SO<sub>4</sub><sup>2-</sup>, NO<sub>3</sub><sup>-</sup>, and NH<sub>4</sub><sup>+</sup> concentrations in rainwater.

Tropospheric NO<sub>2</sub> column densities derived from the CMAQ regional CTM are evaluated with the

Table 1  
EANET site locations and characteristics

ID	Site name	Characteristics	Lat.	Lon.	Height (m)	Country
1	Guanyinqiao	Urban	29.583	106.533	262	China
2	Jinyunshan	Rural	29.817	106.367	800	
3	Shizhan	Urban	34.233	108.950	400	
4	Weishuiyuan	Rural	34.367	108.867	360	
5	Jiwozi	Remote	33.833	108.800	2100	
6	Hongwen	Urban	24.467	118.133	50	
7	Xiaoping	Remote	24.850	118.033	686	
8	Xiang Zhou	Urban	22.267	113.567	40	
9	Zhuxian Caver	Urban	22.200	113.517	45	
10	Rishiri	Remote	45.117	141.233	40	Japan
11	Tappi	Remote	41.250	141.350	105	
12	Sado-seki	Remote	38.250	138.400	110	
13	Happo	Remote	36.683	137.800	1850	
14	Ijira	Rural	35.567	136.700	140	
15	Oki	Remote	36.283	133.183	90	
16	Banryu	Urban	34.667	131.700	60	
17	Yusuhara	Remote	32.733	132.983	225	
18	Hedo	Remote	26.783	128.233	50	
19	Ogasawara	Remote	27.083	142.217	230	
20	Kanghwa	Rural	37.700	126.283	150	South Korea
21	Imsil	Rural	35.600	127.183	0	
22	Cheju	Remote	33.300	126.167	72	
25	Mondy	Remote	51.667	101.000	2000	Russia
26	Irkutsk	Urban	52.233	104.250	400	
27	Listvyanka	Rural	51.850	104.900	700	
28	Ulaanbaatar	Urban	47.900	106.817	1282	Mongolia
29	Terej	Remote	47.983	107.483	1540	
31	Hoa Binh	Rural	20.817	105.333	23	Vietnam
32	Hanoi	Urban	21.017	105.850	5	
30	Mae Hia	Rural	18.767	98.933	350	Thailand
33	Khao Lam Dam	Remote	14.767	98.583	170	
34	Bangkok	Urban	13.767	100.533	2	
36	Patumthani	Rural	14.033	100.767	2	
37	Metro Manila	Urban	14.633	121.067	54	Philippines
38	Los Banos	Rural	14.183	121.250	35	

most recent version of GOME retrieval by Richter et al. (2005) from Bremen University. GOME is an instrument on board the ERS-2 satellite, which was launched by the European Space Agency in April 1995. The GOME instrument observes the atmosphere in nadir view and global coverage is achieved in every 3 days after 43 orbits with a spatial resolution of 40 km latitude by 320 km longitude. Measurements of the satellite instrument GOME have been used to retrieve tropospheric columns of NO<sub>2</sub> based on analysis of observations of solar radiation backscattered from the nadir over the

423–451 nm spectral region where NO<sub>2</sub> has an important absorption feature (Burrows et al., 1999).

### 3. Sulfur dioxide

#### 3.1. Distribution and seasonal variations

Seasonal averaged surface concentrations of SO<sub>2</sub> in winter and in summer are shown in Fig. 2. Large spatial and seasonal variations are found for surface concentrations of SO<sub>2</sub> in East Asia. The seasonal cycle of SO<sub>2</sub> surface concentrations is attributed to

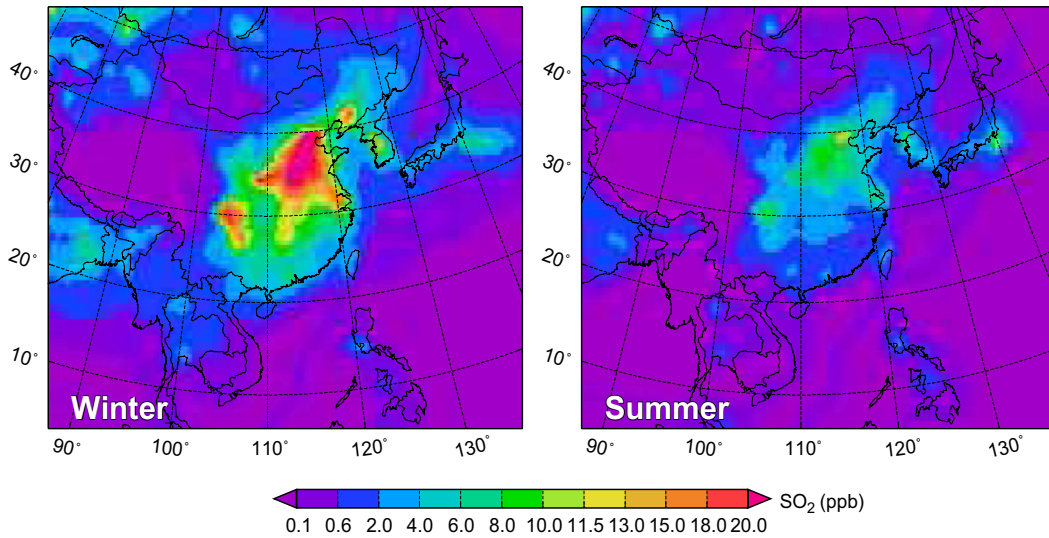


Fig. 2. Distributions of seasonal averaged surface concentration of SO<sub>2</sub> in winter and in summer.

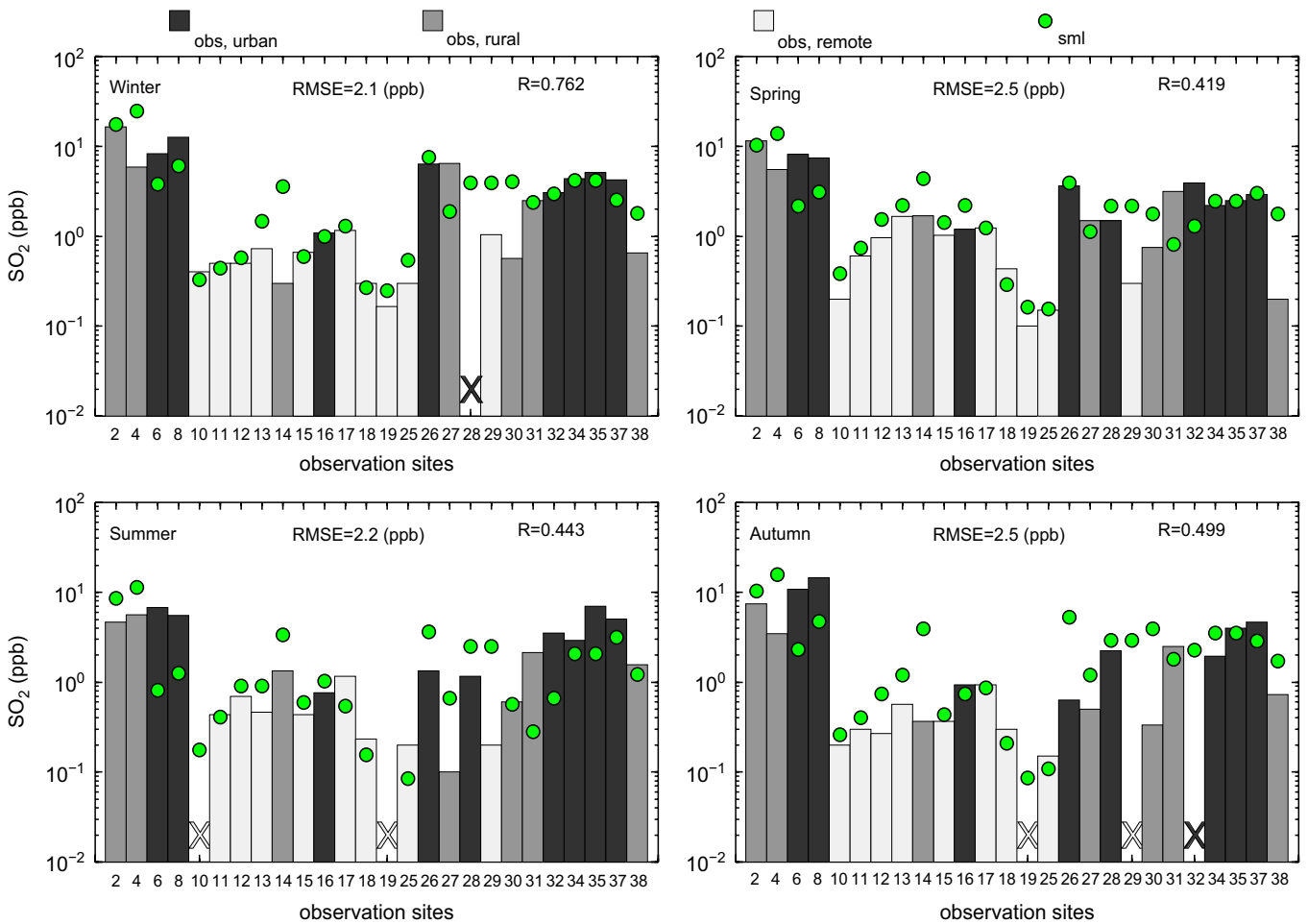


Fig. 3. Comparison between observed (bars) and predicted (circles) SO<sub>2</sub> concentration with 81-km grid spacing for four seasons. RMSE is root mean square error and *R* is correlation coefficient. X indicates that no monitoring data were available.

both variations in emissions and meteorological conditions. In winter due to the highest emissions from residential heating and strong boundary layer

inversion with little mixing and subsidence, surface concentrations of SO<sub>2</sub> reach more than 15 ppb over central eastern China and Sichuan Basin. Large

amount of SO<sub>2</sub> emissions are kept in the near-surface boundary layer over these regions. In summer with strong boundary layer mixing and convection, more SO<sub>2</sub> and its oxidants are transported away or efficiently scavenged by the precipitation. SO<sub>2</sub> concentrations over large areas of eastern China decrease to ~10 ppb in summer.

Fig. 3 compares the modeled and observed results for seasonal averaged concentrations of SO<sub>2</sub> at the EANET monitoring sites. In order to investigate the correlation of model bias with measurement area characteristics, the urban, rural and remote sites are identified with different colors as shown in Fig. 3. The model captures reasonably well the spatial distribution of the high and low SO<sub>2</sub> concentration areas. Underpredictions of SO<sub>2</sub> are found at a few urban sites. The uncertainty in local emission estimates tends to have larger effect on urban areas where the sub-grid variations (e.g. pair sites 28–29 of Mongolia and sites 34–35 of Thailand) may not be resolved in 81-km grid resolution. A systematic overprediction of SO<sub>2</sub> is found at several rural sites, i.e. Weishuishan (site 4) of China, Ijira (site 14) of Japan, Mae Hia (site 30) of Thailand, and Los Banos (site 38) of Philippines. This behavior probably reflects the rather coarse resolution of the model and resultant inability to distinguish the gradient for rural sites that may be located in or nearby grid cells containing large sulfur sources (Carmichael et al., 2007). Overpredictions are also found at two remote mountain sites Happo (site 13) of Japan and Terelj (site 29) of Mongolia. The overprediction at the mountain sites is likely associated with sub-grid scale wind mixing influenced by local topography, which is strongly smoothed for a horizontal resolution of 81 km. This is validated by the comparison at the Happo site between the coarse- and fine-grid simulations shown in Fig. 4.

Observations at Irkutsk (site 27) of Russia clearly show the impact of fossil fuel heating during winter season. It should be noted that SO<sub>2</sub> emissions in Russia from the global data set (Olivier et al., 2005) do not have a seasonal variation. For this reason, SO<sub>2</sub> concentration at Irkutsk is underpredicted in winter, while overpredicted in summer season.

### 3.2. Daily and diurnal variations

Fig. 4 shows the hourly time series of observed and predicted SO<sub>2</sub> mixing ratios at Japanese EANET sites. CMAQ successfully reproduces the

diurnal variations and magnitudes of SO<sub>2</sub> for most days at all sites. Especially with the 27-km grid spacing, model calculation well captures the fine-scale dynamic structures of SO<sub>2</sub> mixing ratios in March at the remote site Oki and the urban site Banryu. For the mountain site Happo, the difference between the coarse- and fine-grid simulations probably reflects the decreasing in local wind mixing associated with smoothing of topography. For the urban site Banryu, SO<sub>2</sub> mixing ratios generally peak at daytime during 16–24 March. The predicted mixing ratios of SO<sub>2</sub> differ appreciably in terms of both magnitudes and diurnal variations with the two horizontal grid spacings, reflecting the sub-grid variations of SO<sub>2</sub> emissions and possible influence of minimum  $K_z$  on nighttime predictions. For the remote sites Sado-seki, Happo, Oki, and Yusuvara, SO<sub>2</sub> concentrations depend primarily on transport processes. The good agreement between predicted and observed results implies that the SO<sub>2</sub> emissions, wind fields, transport processes, and chemical transformations were reasonably well reproduced by the modeling system. Several studies have indicated that middle latitude cyclones forming or intensifying near eastern Asia is a major transport mechanism of Asian pollutants in the springtime (e.g. Carmichael et al., 2003). During March 2001, two eastward traveling low-pressure systems on 17–24 are the dominant meteorological features. The model's ability to capture the variations caused by short-term changes of meteorological conditions is largely attributed to observational data ingested into the reanalysis of the large-scale meteorological fields used for MM5 initialization.

## 4. Tropospheric nitrogen oxides

### 4.1. Comparison with satellite measurements

In contrast to in situ data from EANET, which measures the concentration near the ground, the GOME remote sensing measurements, after correction for vertical sensitivity, yield the column amounts integrated over the troposphere. For comparison, 3-D gridded hourly average NO<sub>2</sub> mixing ratios and MM5-predicted vertically resolved temperature and pressure are used to calculate the NO<sub>2</sub> VCDs in molecule cm<sup>-2</sup> units as follows:

$$\text{VCD} = \sum_{l=1}^8 \frac{P_l \times \Delta Z_l \times A \times [\text{NO}_2]_{\text{ppm},l}}{Rg \times T_l \times 10^6 \times 10^4} \quad (1)$$

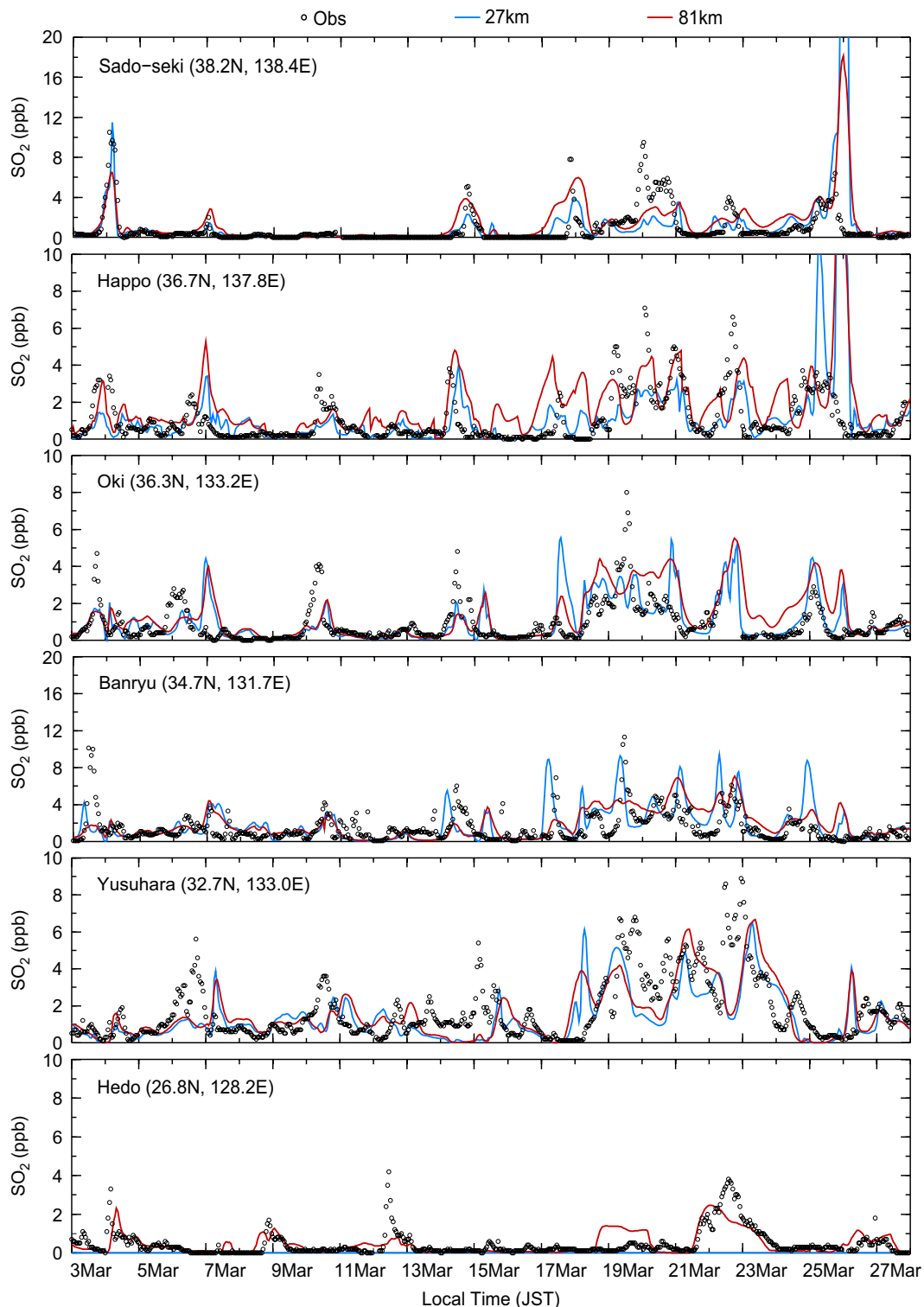


Fig. 4. Hourly time series of observed and predicted SO<sub>2</sub> mixing ratios in March at six EANET sites in Japan.

where  $[\text{NO}_2]_{\text{ppm},l}$  is the NO<sub>2</sub> mixing ratio in ppm in layer  $l$ ,  $\Delta Z_l$  is the height of layer  $l$  in m,  $P_l$  and  $T_l$  are the pressure in Pa and temperature in K, respectively, in layer  $l$ ,  $R_g$  is the gas constant ( $8.34 \text{ J mole}^{-1} \text{ K}^{-1}$ ),  $A$  is the Avogadro's number ( $6.02213 \times 10^{22}$ ).

Monthly averages of model values at 03:00 UTC, which is close to overpass time of the ERS-2 satellite in East Asia, are computed for each grid cell.

Fig. 5 compares satellite measurements of NO<sub>2</sub> column from GOME and the calculated value for

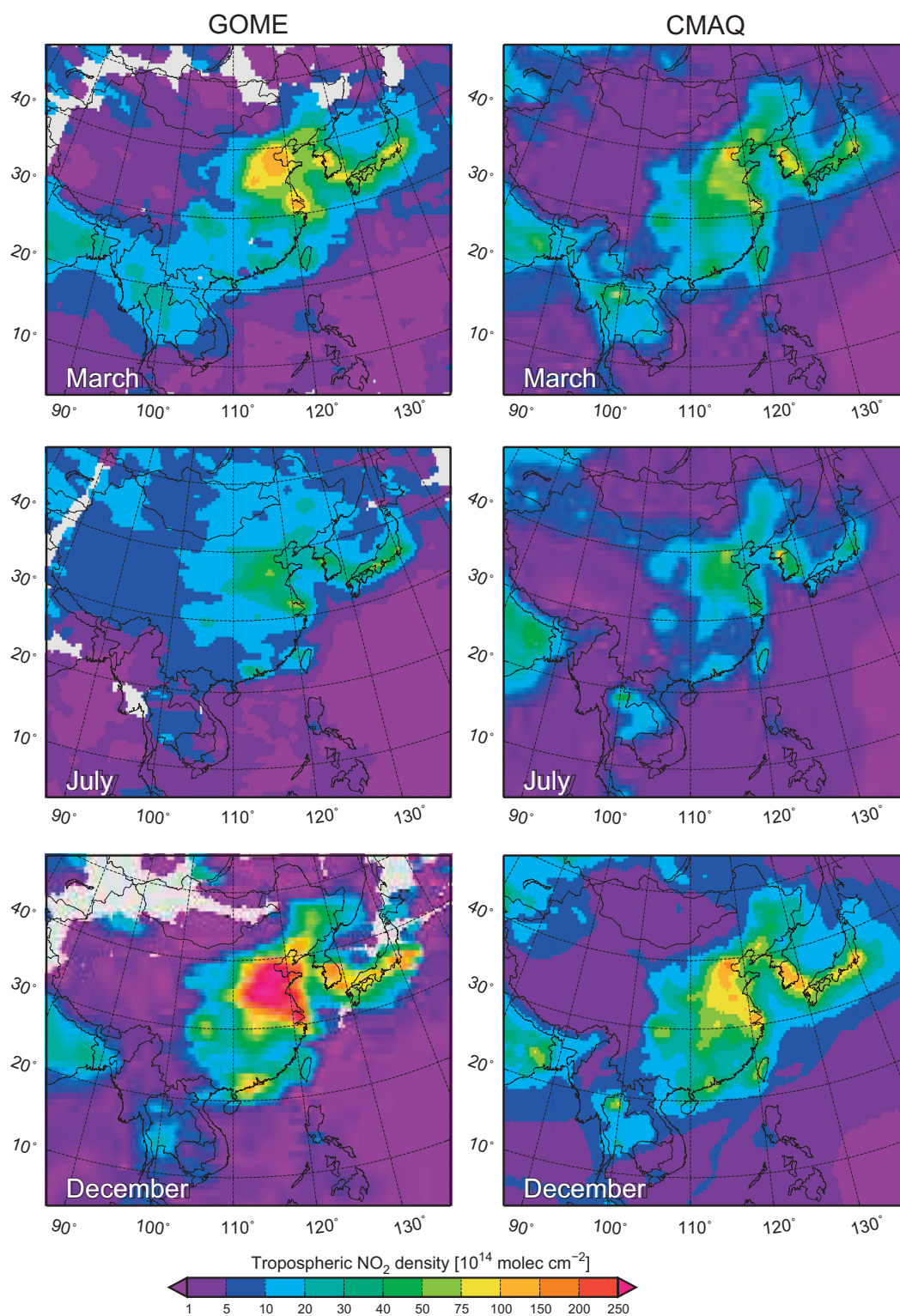


Fig. 5. Satellite measurements of NO<sub>2</sub> columns from GOME (left panels) and the calculated values from CMAQ (right panels) for the selected months, March, July and December.

the selected months March, July, and December. As a result of relatively short lifetime (less than a day) of NO<sub>2</sub> in the PBL, the abundance of NO<sub>2</sub> is

largely controlled by regional emissions and photochemistry while less by long-range transport. The large NO<sub>2</sub> seasonal cycle is explained by the

seasonal variation of the lifetime of  $\text{NO}_x$  in the boundary layer (Kunhikrishnan et al., 2004), related variations in meteorological conditions, and possibly also by higher winter emissions (Jaeglé et al., 2005). Both GOME and model estimated  $\text{NO}_2$  columns highlight the areas of intense pollution in industrialized regions such as central east China, South Korea, and Japan. Regarding the magnitudes of  $\text{NO}_2$  columns in March and December, the discrepancy between model and retrieval is particularly pronounced over central eastern China. However, the summer minimums of the  $\text{NO}_2$  columns over this region are well reproduced, suggesting that the bias over central eastern China cannot be associated with systematic error of the basic inventory data. Below, we analyze sources of discrepancy between model and retrieval in detail for each selected months.

(1) *Sources of discrepancy in July:* As shown in Fig. 5, the model underestimates the GOME retrieval in July by 60% over the remote western China and Mongolia. Martin et al. (2007) estimated that the  $\text{NO}_2$  columns from lightning  $\text{NO}_x$  emissions are lower than  $2.0 \times 10^{14}$  molecule  $\text{cm}^{-2}$  over western China. Soil-biogenic emissions from grassland and scrubland are expected to dominate the  $\text{NO}_2$  sources during the wet season over western China as a result of a low population density. The present study adopted emission estimates of soil-biogenic NO from Yienger and Levy (1995). They constructed a global, temperature and precipitation dependent, empirical model of soil-biogenic  $\text{NO}_x$  emissions. NO emission flux related with N-fertilizer stimulation and rain-induced pulsing, an increase in  $\text{NO}_x$  measured after a shower of rain, have also been considered. Yienger and Levy (1995) introduced a synoptic-scale modeling of rain-induced NO emissions based on daily cumulative precipitation, but did not include the possibility of pulsing in arid scrubland/desert regions. These areas might provide significant short-term pulses when wetted. The Yienger and Levy algorithm may underestimate the magnitude of rain-induced pulsing, especially over arid scrubland/desert regions on mid-latitudes of East Asia.

(2) *Sources of discrepancy in March:* Previous study by Wang et al. (2007) has proposed that the underestimation of  $\text{NO}_2$  sources over central eastern China in springtime may be associated with microbial decomposition of organic waste and with intensive use of chemical fertilizer. Agriculture modeling of Yienger and Levy (1995) did not

resolve different cropping practices and resultant inability to capture the timing of fertilizer application. Yienger and Levy (1995) did not apply any field measurement data obtained from agricultural soils in Asia. The seasonality of agricultural soil emissions is attributed to the timing of fertilizer application and to the influence of seasonal meteorological conditions including temperature and precipitation. Associated with these reasons, they may underestimate NO emissions from agricultural soils in springtime which would partly explain the discrepancy of  $\text{NO}_2$  columns in March over central east China. In addition, biomass burning inventory by van der Werf et al. (2006), which is adopted in this study, relies heavily on satellite data. Compared with the Asian biomass burning inventory by Streets et al. (2003b), this data set may not include smaller agriculture fires (e.g. the burning of crop residues) that cannot be detected from space.

(3) *Sources of discrepancy in December:* In December, CMAQ underestimates the GOME  $\text{NO}_2$  retrieval by a factor of two over central eastern China. The missing of lightning  $\text{NO}_x$  is unlikely responsible for discrepancy in wintertime when lightning activities are weak in this region. Primary reasons for the discrepancy may come from the errors of anthropogenic emission estimates and the GOME retrieval scheme. A growing body of evidence suggests that anthropogenic  $\text{NO}_x$  emissions from eastern China are likely underestimated in the bottom-up emission inventory by Streets et al. (2003a). Recent top-down emission inventories using satellite retrievals (Wang et al., 2007; Jaeglé et al., 2005), and inverse modeling with aircraft measurements (Wang et al., 2004) suggested that errors in the bottom-up combustion sources of  $\text{NO}_x$  from China were likely to be constrained not to exceed 50% seasonally. Except the underestimate of  $\text{NO}_x$  emissions, satellite retrieval might be less reliable in wintertime associated with inadequate treatment of satellite scenes with temporary snow cover (Wang et al., 2007). van Noije et al. (2006) compared three different retrievals by researchers at Bremen University (Richter et al., 2005), Dalhousie University/SAO (Martin et al., 2002), and BIRA/KNMI (Boersma et al., 2004). They found that the differences among three different retrievals are particularly pronounced in wintertime. The Bremen retrieval, which is used in this study, shows 35% higher values over central east China in December than observed in other two retrievals. GOME

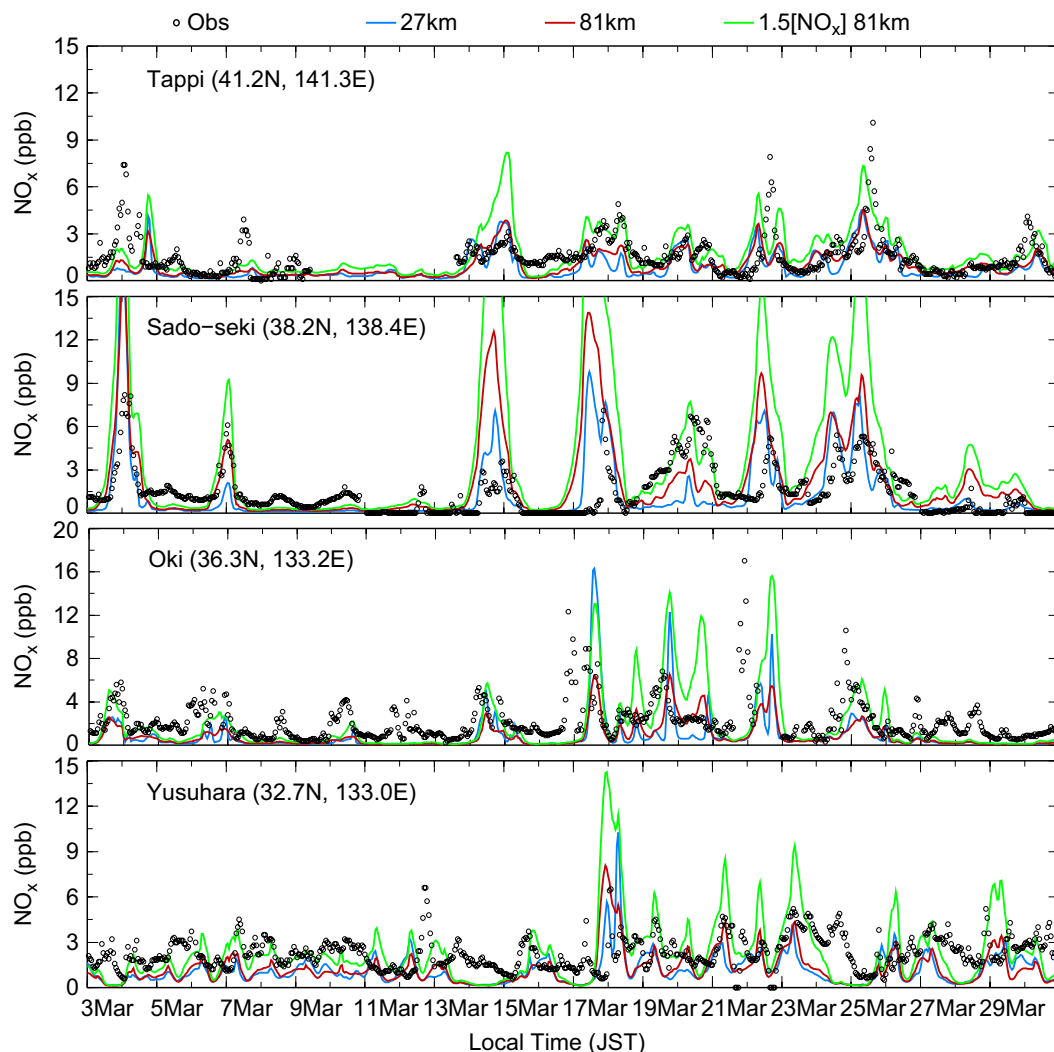


Fig. 6. Hourly time series of observed and predicted  $\text{NO}_x$  mixing ratios in March at four EANET sites in Japan.

retrieval errors have been discussed in detail in several publications (e.g. Boersma et al., 2004).

#### 4.2. Sensitivity studies

To investigate the impact of anthropogenic  $\text{NO}_x$  emissions on tropospheric  $\text{NO}_2$  columns,  $\text{NO}_x$  surface concentrations and  $\text{NO}_3^{-1}$  wet deposition, a new simulation was performed in which  $\text{NO}_x$  emissions were increased by 50% for March. The results are evaluated with the EANET in situ measurements in Japan as well as the GOME data. Fig. 6 shows the hourly time series of observed and predicted  $\text{NO}_x$  mixing ratios in March at the EANET sites from the baseline calculations with both grids and the sensitivity simulation. For Tappi and Sado-seki, the base simulations well reproduces the diurnal variations and magnitudes of  $\text{NO}_x$  on most days. For Oki and Yusu-hara, although most variation signals at the Oki

site are captured, the magnitudes of  $\text{NO}_x$  mixing ratios are systematically underpredicted. The agreement between model and EANET measurements is better in northern Japan than in central south Japan. This spatial behavior is also seen in the comparison for  $\text{NO}_2$  vertical columns and for surface  $\text{NO}_x$  in December (results not shown). Unlike  $\text{SO}_2$ , model calculation with the fine grid spacing does not improve the predictions for  $\text{NO}_x$  very much. A 50% increase of  $\text{NO}_x$  emissions moves the results in the right direction, but does not eliminate the problems. The underpredictions on most days are considerably reduced, but there are some overpredictions of the peak values of  $\text{NO}_x$  mixing ratios on some days. Most daily maximums at Sado-seki are overpredicted by the calculation with 50% increase of  $\text{NO}_x$  emissions.

In response to 50% increase of  $\text{NO}_x$  emissions, the estimated  $\text{NO}_2$  columns increase by 50–80% over eastern China, the Korean Peninsula, and

Japan. The sensitivity results in March agree well with the GOME retrieval over central east China, whereas overpredict the retrieval over central Japan and South Korea by 20–30%. In addition, increasing  $\text{NO}_x$  emissions by 50% causes 30–60% increase of  $\text{NO}_3^-$  wet deposition in March and reduces the model bias approximately by 30% with the EANET measurements in China. Follow up the analysis for March, another new simulation was carried out for December in which  $\text{NO}_x$  emissions were increased by 50% again over central east China whereas by 25% over South Korea and Japan. We find that 50% increase of  $\text{NO}_x$  emissions over central east China in December is not enough to constrain the  $\text{NO}_2$  retrieval over this region. Increasing Japanese emissions by 25% in December well reproduces the GOME retrieval values over Japan. It would be valuable in the future to further explore the impact of increasing  $\text{NO}_x$  emissions on  $\text{O}_3$  formation, and verify the error range of emission estimates when more in situ monitoring data are available and well maintained in China.

## 5. Precipitation and wet deposition

### 5.1. Precipitation fields

The ability of the model to predict concentrations in precipitations and wet depositions is limited by the accuracy of the precipitation fields used in the model. Thus we start with showing the MM5 simulated precipitation fields in winter and in summer (Fig. 7). The seasonality and spatial

distribution of precipitation fields are generally captured by MM5. The predominant weather pattern in the study domain is the Asian monsoon system. In winter, the northwesterly monsoon from the Asian continent to Japan results in heavy snowfalls on the coastal areas of the Japan Sea. The northwesterly monsoon provides a transport path of polluted air mass from the Eurasia, northern China, Korea, and Japan to the eastern Pacific. In summer, the southwesterly monsoonal flow dominates southeast Asia and South China. Asian pollutants are transported along the Pacific Rim toward the northeast.

### 5.2. Comparison with observations

Fig. 8 shows scatter plots of the modeled versus observed results for accumulated precipitation and ionic concentrations in precipitation. The comparison shows that on average MM5 is able to reproduce the precipitation pattern reasonably well with the majority of sites within a factor of 2 of observations. However, the precipitation amounts in the summer months are generally underpredicted within a factor of 5. This may be related to the 81-km horizontal resolution used in MM5 calculations. The precipitation field pattern is very patchy (e.g. influenced by local topography), and the regional scale model is unable to resolve this sub-grid scale distribution.

Non-sea-salt sulfate ( $\text{nssSO}_4^{2-}$ ) has the best agreement against observation among all three ions in precipitation shown in Fig. 8. The majority of

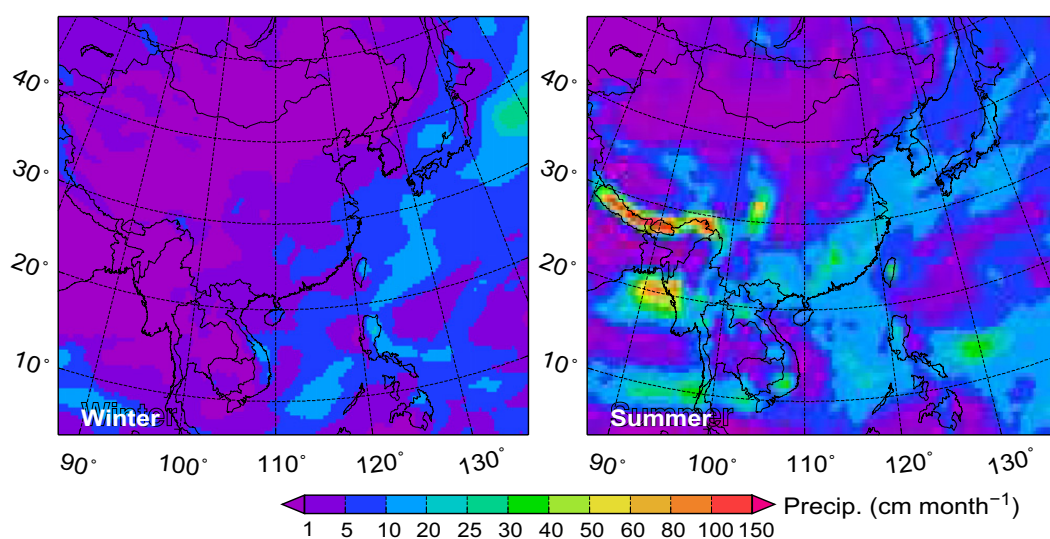


Fig. 7. MM5-predicted distribution fields of monthly accumulated precipitation in winter and in summer.

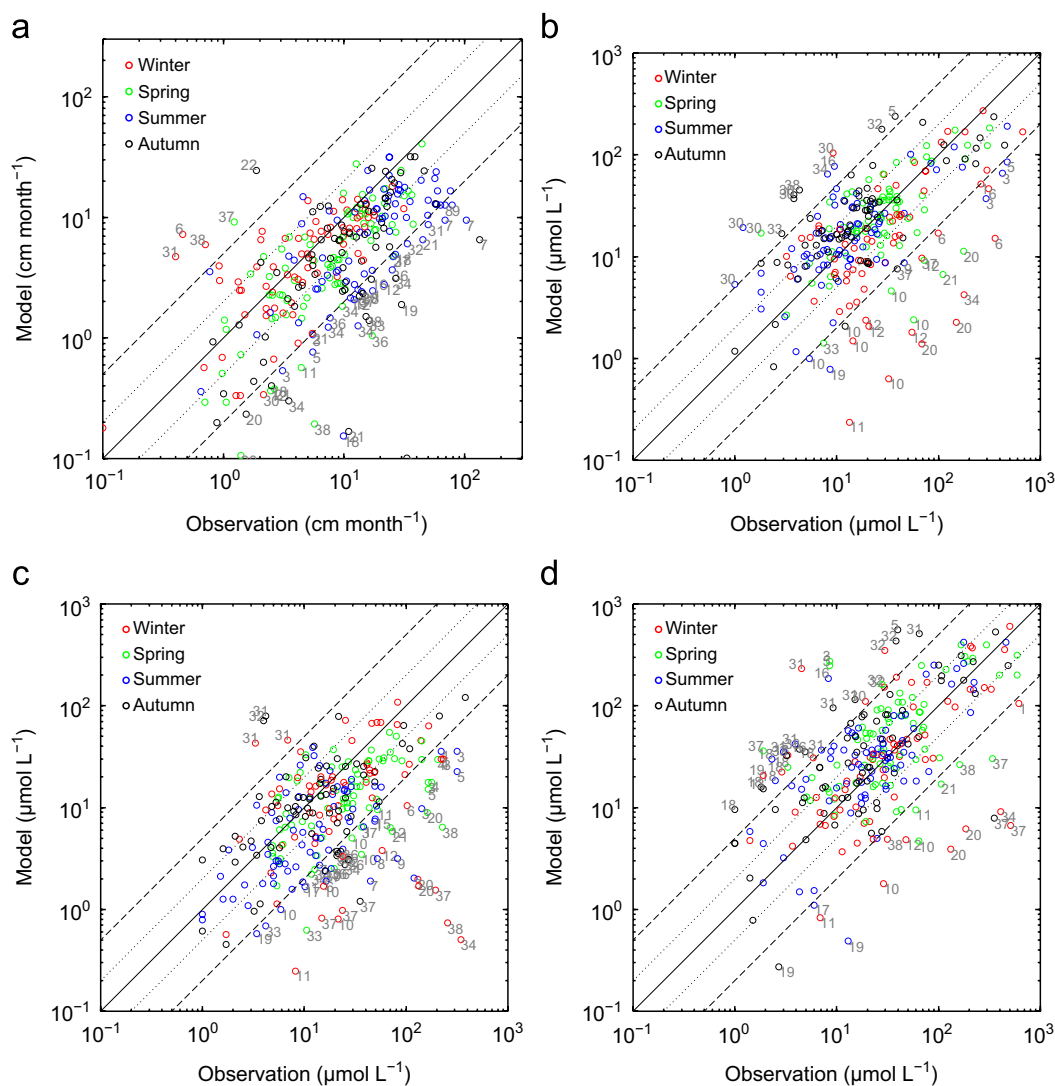


Fig. 8. Scatter plots of modeled versus observed results for (a) accumulated precipitation and concentrations of (b)  $\text{nssSO}_4^{2-}$ , (c)  $\text{NO}_3^-$  and (d)  $\text{NH}_4^+$  in precipitation. Values are monthly pairs with identification color for four seasons. 1:5, 1:2, and 1:1 reference lines are provided. Sites outside the 1:5 reference lines are labeled with identification ID shown in Fig. 1.

Chinese and Japanese sites fall within the reference lines for a factor of 2. In general, the model's lesser ability to predict concentrations in Southeast Asia is related to larger uncertainties in the emission estimates and simulated precipitation fields. During the winter months,  $\text{nssSO}_4^{2-}$ ,  $\text{NO}_3^-$ , and  $\text{NH}_4^+$  in rainwater are found to be systematically under-predicted at the sites located in South Korea (sites 20 and 21) and in northern Japan (sites 10, 11, and 12). Except the errors in predicted precipitation, the wintertime underpredictions of  $\text{nssSO}_4^{2-}$  and  $\text{NO}_3^-$  at these sites are likely caused by the underestimation in residential heating emissions and their seasonality from the local and upper wind regions including central east China, northeast China and Russia. This is consistent with previous discussions about

the underpredictions of wintertime  $\text{SO}_2$  concentrations at the Russian sites and  $\text{NO}_2$  columns over central east China in winter.

Fig. 9 shows the distributions of annual wet deposition of sulfate, nitrate, and ammonium in 2001. The strong continental outflow of Asian pollutants is clearly depicted. These maps provide an Asia-wide perspective on acidic deposition, which is due predominately to sulfur species at present, but with a growing contribution from nitrate. On annual average, the spatial variations and magnitudes of sulfate and ammonium deposition have been well reproduced by the model. Regarding the wet deposition of nitrate, however, there is a moderate underestimation at all EANET sites. In addition to the uncertainties in related meteorology for nitrate

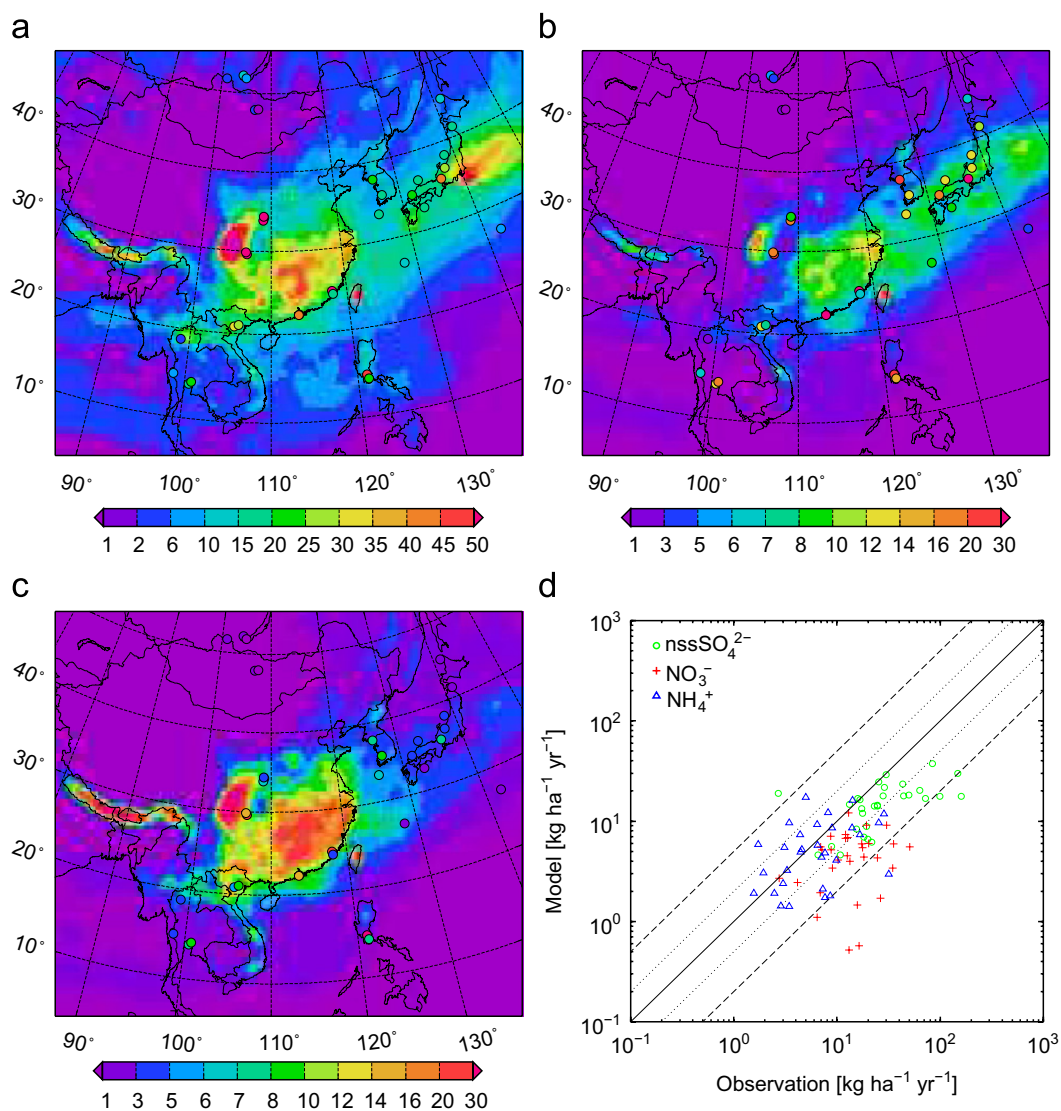


Fig. 9. Annual wet deposition load of sulfate, nitrate, and ammonium in 2001. The filled circles show measurements as observed by the EANET network. (a) nssSO<sub>4</sub><sup>2-</sup>, (b) NO<sub>3</sub><sup>-</sup>, (c) NH<sub>4</sub><sup>+</sup> and (d) scatter plot.

formation, several possible causes may be responsible for the significant underpredictions in nitrate deposition. The primary reason is the underestimates of NO<sub>x</sub> emissions in some parts of East Asia as suggested by the analysis of tropospheric NO<sub>2</sub> columns in Section 4. In addition, some uncertainties exist in the model treatments for governing processes for nitrate formation including thermodynamic equilibrium and gas-to-particle partitioning between gaseous HNO<sub>3</sub> and aerosol nitrate. Gaseous HNO<sub>3</sub> might be dry deposited quickly and thus reduce the wet deposition of NO<sub>3</sub><sup>-</sup>. Previous studies in North America (Yu et al., 2005; Zhang et al., 2006) suggested that the aerosol module of CMAQ has a tendency to underestimate the formation of nitrate aerosol. The aqueous-phase chemistry and some heterogeneous

reactions for nitrate formation, such as HNO<sub>3</sub> uptake by aerosols, are currently not treated in CMAQ (Zhang et al., 2006). There is also high uncertainty in the possibility of heterogeneous reactions of N<sub>2</sub>O<sub>5</sub> on the surface of aerosols to produce HNO<sub>3</sub> (Evans and Jacob, 2005). Finally, Asian emissions of NH<sub>3</sub>, which plays a key role in gas/aerosol partitioning, have not yet been extensively evaluated.

## 6. Conclusions

The CMAQ regional CTM is employed at two horizontal scales to simulate transport and chemistry of acid deposition and related precursors over East Asia using meteorological fields from MM5. We have developed a new emission processing

model to transform available emission data to model resolution, and an interface to link the MOZART global CTM to the CMAQ regional CTM for boundary conditions. Although measurement data in East Asia are relatively scarce, model predictions are compared with the recently available EANET measurements and GOME satellite retrieval to better understand major uncertainties of regional modeling in East Asia.

In evaluating tropospheric NO<sub>2</sub> VCDs, we found that the model significantly underestimated the GOME retrieval over industrial area of eastern China in March and December. Sensitivity simulations with 50% increase of anthropogenic NO<sub>x</sub> emissions agree well the retrieval in March, but are still not enough to constrain the retrieval values in December. The pronounced discrepancy over eastern China is not only due to the uncertainties in the bottom-up emission inventory but also to the reliability of the GOME retrieval scheme in wintertime. The comparison for July also suggests that the soil-biogenic NO emission estimates by Yienger and Levy (1995) need to be reviewed regarding the intensity and timing of fertilizer applications, and the magnitude of rain-induced pulsing during the wet season. Due to the under-predictions of NO<sub>x</sub> and also to the uncertainty in nitrate formation, CMAQ has a tendency to underpredict wet deposition of nitrate observed by the EANET network. More integrated observations of reactive nitrogen gases and aerosols are needed to evaluate the aerosol components of CMAQ.

Regarding the sensitivity of model resolutions, we find that the model calculation with 27-km grid spacing better captures the fine-scale dynamic structure of SO<sub>2</sub> hourly mixing ratios. But even with the 81 km grid spacing, the coarse calculation reasonably well reproduces the magnitudes of seasonal SO<sub>2</sub> at most EANET sites with the root mean square error lower than 2.5 ppb. The coarse calculation also successfully reproduces major spatial and seasonal variations of NO<sub>2</sub> vertical columns observed from space.

Although the sub-grid variations of emissions in urban and rural areas may not be resolved in the coarse resolution, comparison with monthly averaged and hourly observations demonstrates that a computationally efficient model configuration (employing 81 km grid cell and eight layers in the vertical) of the CMAQ regional CTM is capable of representing many of the main features of the distributions of acid precursors and deposition.

Thus, we employed the model to calculate the S/R relationships of acid deposition on regional scale as presented in Lin et al. (2008b).

### Acknowledgments

This research has been supported by Japan International Cooperation Agency and Grants-in-Aid for Scientific Research, Japan Society for the Promotion of Science (19106008). We thank Dr. Richter at Bremen University for providing the GOME NO<sub>2</sub> retrieval, EANET for providing surface measurements, and two anonymous reviewers for helpful suggestions.

### References

- Bey, I., Jacob, D.J., Logan, J.A., Yantosca, R.M., 2001. Asian chemical outflow to the Pacific in spring: origins, pathways, and budgets. *Journal of Geophysical Research* 106 (D19), 23097–23113.
- Binkowski, F.S., Roselle, S.J., 2003. Models-3 community multiscale air quality (CMAQ) model aerosol component—1. Model description. *Journal of Geophysical Research* 108 (D6).
- Boersma, K.F., Eskes, H.J., Brinksma, E.J., 2004. Error analysis for tropospheric NO<sub>2</sub> retrieval from space. *Journal of Geophysical Research* 109, D04311.
- Burrows, J., Weber, M., Buchwitz, M., Rozanov, V.V., Ladstätter-Weißmayer, A., Richter, A., DeBeek, R., Hoogen, R., Brmstedt, K., Eichmann, K., 1999. The global ozone monitoring experiment (GOME): mission concept and first scientific results. *Journal of the Atmospheric Sciences* (56), 151–175.
- Byun, D.W., Ching, J.K.S. (Eds.), 1999. *Science Algorithms of the EPA Models-3 Community Multi-scale Air Quality (CMAQ) Modeling System*. NERL, Research Triangle Park, NC.
- Byun, D.W., Schere, K.L., 2006. Review of the governing equations, computational algorithms, and other components of the models-3 community multiscale air quality (CMAQ) modeling system. *Applied Mechanics Reviews* (59), 51–77.
- Carmichael, G.R., et al., 2003. Regional-scale chemical transport modeling in support of the analysis of observations obtained during the TRACE-P experiment. *Journal of Geophysical Research* 108 (D21).
- Carmichael, G.R., et al., 2007. MICS-Asia II: the model intercomparison study for Asia phase II: methodology and overview of findings. *Atmospheric Environment*, in press, doi:10.1016/j.atmosenv.2007.04.007.
- Carter, W., 2000. Implementation of the sarp-99 chemical mechanism into the models-3 framework. Report to the United States Environmental Protection Agency, January 29, 2000.
- Colella, P., Woodward, P.R., 1984. The piecewise parabolic method (PPM) for gas-dynamical simulations. *Journal of Computational Physics* (54), 174–201.

- Dentener, F.J., Carmichael, G., Zhang, Y., Lelieveld, J., Crutzen, P.J., 1993. Reaction of  $\text{N}_2\text{O}_5$  on tropospheric aerosols: impact on the global distributions of  $\text{NO}_x$ ,  $\text{O}_3$ , and OH. *Journal of Geophysical Research* 98, 7149–7163.
- EANET, 2002. Data Report on the Acid Deposition in the East Asian Region 2001. Available at (<http://www.eanet.cc/product.html>), Network Center for EANET.
- Evans, M.J., Jacob, D.J., 2005. Impact of new laboratory studies of  $\text{N}_2\text{O}_5$  hydrolysis on global model budgets of tropospheric nitrogen oxides, ozone, and OH. *Geophysical Research Letter* 32, L09813.
- Gery, M., Whitten, G.Z., Killus, J.P., Dodge, M.C., 1989. A photochemical kinetics mechanism for urban and regional scale computer modeling. *Journal of Geophysical Research* 94, 925–956.
- Grell, G.A., Dudhia, J., Stauffer, D.R., 1994. A description of the fifth-generation Penn State/NCAR mesoscale model (MM5). NCAR Technical Note NCAR/TN-398+STR, 117pp.
- Holloway, T., et al., 2007. MICS-Asia II: impacts of global emissions on regional air quality in Asia. *Atmospheric Environment*, in press, doi:10.1016/j.atmosenv.2007.10.022.
- Hong, S.Y., Pan, H.L., 1996. Nonlocal boundary layer vertical diffusion in a medium-range forecast model. *Monthly Weather Review* 124, 2322–2339.
- Horowitz, L.W., Walters, S., Mauzerall, D.L., Emmons, L.K., Rasch, P.J., Granier, C., Tie, X.X., Lamarque, J.F., Schultz, M.G., Tyndall, G.S., Orlando, J.J., Brasseur, G.P., 2003. A global simulation of tropospheric ozone and related tracers: description and evaluation of MOZART, version 2. *Journal of Geophysical Research* 108 (D24).
- Jaeglé, L., Steinberger, L., Martin, R.V., Chance, K., 2005. Global partitioning of  $\text{NO}_x$  sources using satellite observations: relative roles of fossil fuel combustion, biomass burning and soil emissions. *Faraday Discussions* 130, 407–423.
- Kajino, M., Ueda, H., Satsumabayashi, H., An, J.L., 2004. Impacts of the eruption of Miyakejima volcano on air quality over far east Asia. *Journal of Geophysical Research* 109 (D21).
- Kazahaya, K., Shinohara, H., Uto, K., Odai, M., Nalkahori, Y., Mori, H., Iino, H., Miyashita, M., Hirabayashi, J., 2004. Gigantic  $\text{SO}_2$  emission from Miyakejima volcano, Japan, caused by caldera collapse. *Geology* 32 (5), 425–428.
- Kunhikrishnan, T., Lawrence, M.G., von Kuhlmann, R., Richter, A., Ladstatter-Weissenmayer, A., Burrows, J.P., 2004. Analysis of tropospheric  $\text{NO}_x$  over Asia using the model of atmospheric transport and chemistry (MATCH-MPIC) and GOME-satellite observations. *Atmospheric Environment* 38 (4), 581–596.
- Lin, M., Holloway, T., Oki, T., Streets, D.G., 2008a. Sensitivity of regional ozone predictions in East Asia to photochemistry and boundary conditions: A multiscale study coupling regional and global chemical transport models. Manuscript in preparation for *Atmospheric Chemistry and Physics*.
- Lin, M., Oki, T., Bengtsson, M., Kanae, S., Holloway, T., Streets, D.G., 2008b. Long-range transport of acidifying substances in Asia—part II: source–receptor relationships. *Atmospheric Environment*, in press, doi:10.1016/j.atmosenv.2008.03.039.
- Liu, H.Y., Jacob, D.J., Chan, L.Y., Oltmans, S.J., Bey, I., Yantosca, R.M., Harris, J.M., Duncan, B.N., Martin, R.V., 2002. Sources of tropospheric ozone along the Asian Pacific Rim: an analysis of ozonesonde observations. *Journal of Geophysical Research* 107 (D21).
- Martin, R.V., Chance, K., Jacob, D.J., Kurosu, T.P., Spurr, R.J.D., Bucseles, E., Gleason, J.F., Palmer, P.I., Bey, I., Fiore, A.M., Li, Q.B., Yantosca, R.M., Koelemeijer, R.B.A., 2002. An improved retrieval of tropospheric nitrogen dioxide from GOME. *Journal of Geophysical Research* 107 (D20).
- Martin, R.V., Sauvage, B., Folkins, I., Sioris, C.E., Boone, C., Bernath, P., Ziemke, J., 2007. Space-based constraints on the production of nitric oxide by lightning. *Journal of Geophysical Research* (112), D09309, doi:10.1029/2006JD007831.
- Naja, M., Akimoto, H., 2004. Contribution of regional pollution and long-range transport to the Asia-Pacific region: analysis of long-term ozonesonde data over Japan. *Journal of Geophysical Research* 109 (D21).
- Olivier, J., Peters, J., Granier, C., Petron, G., Müller, J.F., Wallens, S., 2003. Present and future surface emissions of atmospheric compounds, POET (Precursors of Ozone and their Effects in the Troposphere). Report No. 2 (EU project EVK2-1999-00011, 2003).
- Olivier, J.G.J., Aardenne, J.A.V., Dentener, F., Ganzeveld, L., Peters, J.A.H.W., 2005. Recent trends in global greenhouse gas emissions: regional trends and spatial distribution of key sources. In: *Non-CO<sub>2</sub> Greenhouse Gases (NCGG-4)*. A. van Amstel (coord.), Millpress, Rotterdam, pp. 325–330, ISBN 90 5966 043 9.
- Richter, A., Burrows, J.P., Nuss, H., Granier, C., Niemeier, U., 2005. Increase in tropospheric nitrogen dioxide over China observed from space. *Nature* 437 (7055), 129–132.
- Seto, S., Nakamura, A., Noguchi, I., Ohizumi, T., Fukuzaki, N., Toyama, S., Maeda, M., Hayashi, K., Hara, H., 2002. Annual and seasonal trends in chemical composition of precipitation in Japan during 1989–1998. *Atmospheric Environment* 36 (21), 3505–3517.
- Streets, D.G., Bond, T.C., Carmichael, G.R., Fernandes, S.D., Fu, Q., He, D., Klimont, Z., Nelson, S.M., Tsai, N.Y., Wang, M.Q., Woo, J.H., Yarber, K.F., 2003a. An inventory of gaseous and primary aerosol emissions in Asia in the year 2000. *Journal of Geophysical Research* 108 (D21).
- Streets, D.G., Yarber, K.F., Woo, J.H., Carmichael, G.R., 2003b. Biomass burning in Asia: annual and seasonal estimates and atmospheric emissions. *Global Biogeochemical Cycles* 17 (4).
- van der Werf, G.R., Randerson, J.T., Giglio, L., Collatz, G.J., Kasibhatla, P.S., Arellano, A.F., 2006. Interannual variability in global biomass burning emissions from 1997 to 2004. *Atmospheric Chemistry and Physics* 6, 3423–3441.
- van Noije, T.P.C., et al., 2006. Multi-model ensemble simulations of tropospheric  $\text{NO}_2$  compared with GOME retrievals for the year 2000. *Atmospheric Chemistry and Physics* 6, 2943–2979.
- Wang, Y., Zhuang, G.S., Zhang, X.Y., Huang, K., Xu, C., Tang, A.H., Chen, J.M., An, Z.S., 2006. The ion chemistry, seasonal cycle, and sources of  $\text{PM}_{2.5}$  and TSP aerosol in Shanghai. *Atmospheric Environment* 40 (16), 2935–2952.
- Wang, Y.X., McElroy, M.B., Wang, T., Palmer, P.I., 2004. Asian emissions of CO and  $\text{NO}_x$ : constraints from aircraft and Chinese station data. *Journal of Geophysical Research* 109, D24304.
- Wang, Y.X., McElroy, M.B., Martin, R.V., Streets, D.G., Zhang, Q., Fu, T.M., 2007. Seasonal variability of  $\text{NO}_x$  emissions over east China constrained by satellite observations:

- implications for combustion and microbial sources. *Journal of Geophysical Research* 112 (D6).
- Xie, M., 2002. The basic feature research of acid rain pollution in Guangzhou area between 1996 and 2000. *Research of Environmental Science* 15 (1), 31–33 (in Chinese).
- Yienger, J.J., Levy, H., 1995. Empirical model of global soil-biogenic  $\text{NO}_x$  emissions. *Journal of Geophysical Research* 100, 1447–1464.
- Yu, S.C., Dennis, R., Roselle, S., Nenes, A., Walker, J., Eder, B., Schere, K., Swall, J., Robarge, W., 2005. An assessment of the ability of three-dimensional air quality models with current thermodynamic equilibrium models to predict aerosol  $\text{NO}_3$ . *Journal of Geophysical Research* 110 (D7).
- Zhang, Y., Liu, P., Queen, A., Misenis, C., Pun, B., Seigneur, C., Wu, S.Y., 2006. A comprehensive performance evaluation of MM5-CMAQ for the summer 1999 southern oxidants study episode—part II: gas and aerosol predictions. *Atmospheric Environment* 40 (26), 4839–4855.